

A Comparative Study of Interval Type-2 and Type-1 Fuzzy Sliding Mode in Controlling DFIG-Based Wind Energy Conversion System



I. Allali*, B. Dehiba

IRECOM-laboratory, University Djillali Liabes of Sidi Bel-Abbes, Algeria.



ABSTRACT: This paper explores the use of Interval Type-2 Fuzzy Sliding Mode Control (IT2-FSMC) for managing a double-fed induction generator (DFIG) in wind energy systems. By combining sliding mode control with fuzzy logic, the method effectively mitigates model uncertainty and reduces chatter, a prevalent issue in variable-structure systems. The paper includes a thorough comparison with type-1 fuzzy sliding mode control (T1-FSMC). The proposed control techniques are tested under various conditions, such as changing wind speed and parameter variations, to evaluate their performance. Simulation results show that IT2-FSMC outperforms T1-FSMC in terms of rise time and reference tracking. IT2-FSMC also significantly reduces the integral of the square error (ISE), integral of the absolute error (IAE), integral time absolute error (ITAE), and integral time square error (ITSE), and achieves the lowest values for both active and reactive power, while reducing the current harmonic distortion (THD) to 80.72%. Simulations were performed using MATLAB/Simulink software.

KEYWORDS: Doubly fed induction generator (DFIG), Wind power, Sliding mode control, Interval type-2 fuzzy Logic control, Type-1 fuzzy logic control.

[Received Aug. 18, 2025; Revised Mar. 12, 2025; Accepted April 13, 2025] Print ISSN: 0189-9546 | Online ISSN: 2437-2

Nomenclature		
MPPT	Maximum power point tracking	P_s, Q_s Active and reactive stator power
MF	Membership function	s, r Stator and rotor subscripts
IAE	Integral of the absolute error	V, I, ϕ Voltage/ Current/ Flux variables
ISE	Integral of the square error	R_s, R_r Stator, rotor resistance
ITSE	Integral time square error	L_s, L_r Stator, rotor inductance
ITAE	Integral time absolute error	M Mutual inductance
THD	Total Harmonic Distortion	ω, ω_s Mechanical rotor frequency/ Electrical stator frequency
IT2-FSMC	Interval type-2 fuzzy sliding mode control	C_p Power coefficient
T1-FSMC	Type-1 fuzzy sliding mode control	C_f, J_T Viscous coefficient/ Inertia moment
		β, λ Pitch angle/ Speed ratio

I. INTRODUCTION

Wind energy has grown significantly over the past decade, proving to be both sustainable and environmentally beneficial (Xiong et al., 2021; Heier, 2014). Rising fuel costs and increasing public concern about the environmental impact of thermal and nuclear power have spurred interest in wind power generation systems (WPGS) as a leading renewable energy option. Globally, wind power capacity has exceeded the gigawatt (GW) mark, with larger wind power plants in the pipeline (Yin et al., 2016; Scarabaggio et al., 2021). Most wind turbines currently use a DFIG for its benefits, such as variable speed capability ($\pm 30\%$ around synchronous speed), independent control of active and reactive power (P_s and Q_s), reduced noise and mechanical stress, enhanced power quality, and low cost (Khan et al., 2020).

Controlling a Doubly Fed Induction Machine (DFIM) system requires classical methods, including proportional, integral, and derivative actions. A comprehensive understanding of system parameters and the ability to respond effectively are crucial for successful implementation. However, errors and inaccuracies in knowledge are common, and the interconnected nature of system variables complicates control (Kaloi et al., 2019). This issue can be addressed with nonlinear techniques such as sliding mode (Amira et al., 2020) and fuzzy logic (Hemeyine et al., 2020).

Sliding mode control (SMC) is a reliable control technique for both linear and nonlinear systems because it can easily handle parameter changes, external disturbances, and unmodeled dynamics (Mousavi et al., 2022). The main drawback of this approach is the higher switching frequency caused by control switching when the system state crosses the

*Corresponding author: izzeddine.allali@univ-sba.dz

sliding surface, which leads to chattering. Chattering can induce high frequency unmodeled modes, which is detrimental to the nonlinear control system (Mancini et al., 2020). In this particular problem, fuzzy mode control is used instead of discontinuous control. The goal of this research is to design a control system that is immune to coupling effects, can handle parametric uncertainties, and can dampen disturbances caused by speed changes.

Professor Zadeh first introduced fuzzy theory in 1965. A steam engine and boiler system were controlled by linguistic rules using the Mamdani fuzzy inference system. Fuzzy logic uses natural language to express if-then rules (Hemeyine et al., 2020). However, type-1 fuzzy logic systems (T1FLS) have limitations in representing uncertainties and nonlinearities due to their crisp membership levels of input values. This led to the development of type-2 fuzzy logic systems (T2FLS), an advanced form originally proposed by L. Zadeh. In recent years, researchers have focused on T2FLS and established its theoretical foundations (Hassani and Zarei, 2015; Kheir-Saadaoui et al., 2019; Acikgoz et al., 2017). The key feature of T2FLS is the Footprint of Uncertainty (FOU), which effectively accounts for uncertainties and nonlinearities. Numerous studies have shown that T2FLS is significantly more robust than T1FLS in dealing with these challenges (Yan et al., 2024).

This paper is structured as follows: Section 2 Theoretical Analysis. Section 3 presents the methodology. In Section 4, it compares the performance and reliability of IT2-FSMC with T1-FSMC. The last part focuses on the conclusion.

II. THEORETICAL ANALYSIS

The wind conversion system is shown in Fig 1.

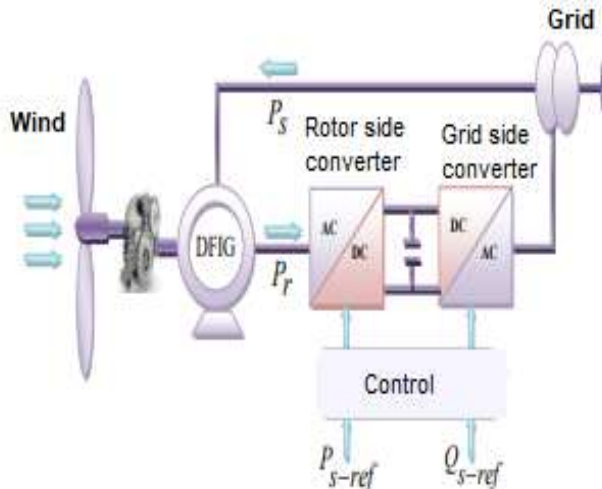


Figure 1: Synoptic diagram of the wind system.

A. Modeling the Turbine

The equation represents the relationship between wind speed (v) and turbine energy recovery from wind kinetic energy (P_m) (Sahri et al., 2021; Shuaibu et al., 2021).

$$P_m = \frac{1}{2} \rho \pi R^2 v^3 C_p(\lambda, \beta) \quad (1)$$

Where (ρ) is the air density (1.225 kg/m^3), (R) is the turbine blade radius, (C_p) is the power coefficient dependent on the pitch angle (β), and (λ) is the speed ratio, provided by the equation.

$$\lambda = \frac{\Omega R}{v} \quad (2)$$

The turbine rotor's angular speed is represented by Ω . The power coefficient C_p has a theoretical maximum of 0.593 (Adeyanju, 2023). Turbine torque is the ratio of transmitted power and rotor speed Ω (Sahri et al., 2021; Shuaibu et al., 2021):

$$T_m = \frac{P_m}{\Omega} = \frac{1}{2\lambda} \rho \pi R^3 v^2 C_p(\lambda, \beta) \quad (3)$$

The power coefficient C_p is influenced by the pitch angle β and the tip speed ratio λ (Milles et al., 2024; Okedu. et al., 2021).

$$C_p(\lambda, \beta) = c_1 \left(\frac{c_2}{\lambda_i} - c_3 \beta - c_4 \right) e^{-\frac{c_5}{\lambda_i}} + c_6 \lambda \quad (4)$$

With: $c_1 = 0.5176$, $c_2 = 116$, $c_3 = 0.4$, $c_4 = 5$, $c_5 = 21$, $c_6 = 0.0068$.

Where λ_i is given by the equation (Milles et al., 2024; Okedu. et al., 2021):

$$\lambda_i = \left[\frac{1}{(\lambda + 0.08\beta)} - \frac{0.35}{(\beta^3 + 1)} \right]^{-1} \quad (5)$$

Optimizing wind turbine efficiency requires maximum power point tracking (MPPT) control to regulate speed, particularly at low wind speeds. This is done by maintaining the optimal value of $\lambda_{opt} = 8.1$, assuming $\beta = 0$ (Sahri et al., 2021; Hemeyine et al., 2020), to achieve the maximum power coefficient C_{p-max} . The electromagnetic torque T_m of the DFIG turbine must be adjusted to keep the DFIG speed at the reference value (Mousa et al., 2020; Kadri et al., 2020).

$$T_m = \frac{\rho c_{p-max}}{2} \frac{R_t^5}{\lambda_{opt}^3} \pi \frac{R_t}{G} \Omega_{mec}^2 \quad (6)$$

Excessive wind speeds can harm turbine structures, necessitating a limit to the rated speed. The pitch controller must monitor the turbine's power output and adjust the blade pitch to optimize performance in varying wind conditions (Mousa et al., 2020; Hemeyine et al., 2020).

B. Modeling of the DFIG

The following equations characterize the DFIG model in the d-q reference frame (Hemeyine et al., 2020).

$$\begin{cases} V_{sd} = R_s I_{sd} + \frac{d\phi_{sd}}{dt} - \omega_s \phi_{sq} \\ V_{sq} = R_s I_{sq} + \frac{d\phi_{sq}}{dt} + (\omega_s - \omega_r) \phi_{sd} \\ V_{rd} = R_r I_{rd} + \frac{d\phi_{rd}}{dt} - \omega_s \phi_{rq} \\ V_{rq} = R_r I_{rq} + \frac{d\phi_{rq}}{dt} + (\omega_s - \omega_r) \phi_{rd} \end{cases} \quad (7)$$

Rotor and stator fluxes are expressed as follows.

$$\begin{cases} \phi_{sd} = L_s I_{sd} + M I_{rd} \\ \phi_{sq} = L_s I_{sq} + M I_{rq} \\ \phi_{rd} = L_r I_{rd} + M I_{sd} \\ \phi_{rq} = L_r I_{rq} + M I_{sq} \end{cases} \quad (8)$$

The mechanical equation of the system is

$$J_T \frac{d\Omega_{mec}}{dt} = \Gamma_{em} = \Gamma_r + C_f \Omega_{mec} + \quad (9)$$

Torque can be expressed as:

$$\Gamma_{em} = p \frac{M}{L_s} (\phi_{sd} I_{rq} - \phi_{sq} I_{rd}) \quad (10)$$

By independently utilizing stator flux orientation for energetic and reactive power control, we may simplify the regulation of the DFIG. Ensure that the stator flux is parallel to the d-axis of the rotating frame. This work will achieve this orientation with a real DFIG model without neglecting the stator resistance (Chakib et al., 2020).

$$\Phi_{sd} = \phi_s \quad \text{et} \quad \phi_{sq} = 0 \quad (11)$$

The equation (8) of the flux becomes as follows.

$$\begin{cases} \phi_{sd} = L_s I_{sd} + M I_{rd} \\ 0 = L_s I_{sq} + M I_{rq} \end{cases} \quad (12)$$

In addition, the stator voltage equations are simplified as follows.

$$V_{sd} = 0, \quad V_{sq} = V_s = \omega_s \phi_s \quad (13)$$

The stator power is controlled by the rotor voltages V_{rd} and V_{rq} , allowing independent control of active and reactive power. In the d-q reference frame, the power can be expressed as:

$$\begin{cases} P_s = V_{sd} I_{sd} + V_{sq} I_{sq} = -V_s \frac{M}{L_s} I_{rq} \\ Q_s = V_{sq} I_{sd} - V_{sd} I_{sq} = -V_s \frac{M}{L_s} I_{rd} + V_s \frac{\phi_s}{L_s} \end{cases} \quad (14)$$

$$\begin{cases} V_{rd} = R_r I_{rd} + \left(L_r - \frac{M^2}{L_s}\right) \frac{dI_{rd}}{dt} - g \omega_s \left(L_r - \frac{M^2}{L_s}\right) I_{rq} \\ V_{rq} = R_r I_{rq} + \left(L_r - \frac{M^2}{L_s}\right) \frac{dI_{rq}}{dt} + g \omega_s \left(L_r - \frac{M^2}{L_s}\right) I_{rd} + g \frac{M V_s}{L_s} \end{cases} \quad (15)$$

C. Sliding Mode Control

SMC has seen significant success in recent years. This is due to its ease of implementation and its ability to withstand system uncertainties and external disturbances that may affect the process. Sliding mode control involves first mapping the states of the system within a carefully chosen region and then devising a control rule that ensures the system remains consistently within this region (Slotine et al., 1991; Bühler, 1986). Sliding mode control consists of three distinct steps:

1) Choice of switching surface

The following form is used to represent a nonlinear system:

$$\dot{X} = f(X, t) + g(X, t) u(X, t) \quad (16)$$

Where $X \in \mathfrak{R}^n$ is the state vector, $u \in \mathfrak{R}^m$ is the control vector, $f(X, t) \in \mathfrak{R}^n$, $g(X, t) \in \mathfrak{R}^{n \times m}$

To get the sliding surface, we use the generic equation provided by J.J. Slotine, as stated in (Bühler, 1986).

$$S(X) = \left(\frac{\partial}{\partial t} + \lambda\right)^{n-1} e(X) \quad (17)$$

Where $e(X) = X^d - X$.

e : error on the controlled variable - λ : positive coefficient-
 n : system order.

2) Convergence condition

The area becomes attractive and invariant when the convergence condition is met, which is specified by the Lyapunov equation (Bühler, 1986).

$$S(X) \dot{S}(X) \leq 0 \quad (18)$$

3) Computation of the control

The relationship defines the control algorithm.

$$u = u^{eq} + u^n \quad (19)$$

Where u : is the control vector, u^{eq} : is the equivalent control vector, u^n : is the switching part of the control (the correction factor).

J. J. Slotine suggested a method to lessen the unwanted chattering phenomena by adding a boundary layer with a width of ϕ on both sides of the switching surface (Slotine et al., 1991). Next, u^n is determined by:

$$u^n = K \text{sat}(S(X)/\phi) \quad (20)$$

Where ϕ is the boundary layer width and $\text{sat}(S(X)/\phi)$ is the suggested saturation function, K is the controller gain.

4) Power control

For power control, $n=1$. The expression for the active and reactive power control surface becomes:

$$\begin{cases} s(P_s) = (P_s^{ref} - P_s) \\ s(Q_s) = (Q_s^{ref} - Q_s) \end{cases} \quad (21)$$

A surface's derivative is:

$$\begin{cases} \dot{s}(P_s) = (\dot{P}_s^{ref} - \dot{P}_s) \\ \dot{s}(Q_s) = (\dot{Q}_s^{ref} - \dot{Q}_s) \end{cases} \quad (22)$$

The power expression (Equation 14) is replaced by

$$\begin{cases} \dot{s}(P_s) = (\dot{P}_s^{ref} + V_s \frac{M}{L_s} \dot{I}_{rq}) \\ \dot{s}(Q_s) = \dot{Q}_s^{ref} - \left(-V_s \frac{M}{L_s} \dot{I}_{rd}\right) \end{cases} \quad (23)$$

We use equation (15) to get the current from the voltage equation.

$$\begin{cases} \dot{s}(P_s) = \dot{P}_s^{ref} + V_s \frac{M}{\sigma L_r L_s} (V_{rq} - R_r I_{rq} - g \omega_s \sigma L_r I_{rd} - g \frac{M V_s}{L_s}) \\ \dot{s}(Q_s) = \dot{Q}_s^{ref} + V_s \frac{M}{\sigma L_r L_s} (V_{rd} - R_r I_{rd} + g \omega_s \sigma L_r I_{rq}) \end{cases} \quad (24)$$

$$\begin{cases} V_{qr} = V_{qr}^{eq} + V_{qr}^n \\ V_{rd} = V_{rd}^{eq} + V_{rd}^n \end{cases} \quad (25)$$

$$\begin{cases} \dot{s}(P_s) = \dot{P}_s^{ref} + V_s \frac{M}{\sigma L_r L_s} ((V_{rq}^{eq} + V_{rq}^n) - R_r I_{rq} - g \omega_s \sigma L_r I_{rd} - g \frac{M V_s}{L_s}) \\ \dot{s}(Q_s) = \dot{Q}_s^{ref} + V_s \frac{M}{\sigma L_r L_s} ((V_{rd}^{eq} + V_{rd}^n) - R_r I_{rd} + g \omega_s \sigma L_r I_{rq}) \end{cases} \quad (26)$$

Where: $\sigma = 1 - (L_m^2 / L_s L_r)$ is the leakage factor, and g represents the slip of the induction machine. During the sliding mode and steady state, we have:

$$\begin{cases} s(P_s) = 0, \dot{s}(P_s) = 0, V_{rq}^n = 0 \\ s(Q_s) = 0, \dot{s}(Q_s) = 0, V_{rd}^n = 0 \end{cases} \quad (27)$$

The equivalent control variables V_{qr}^{eq} and V_{rd}^{eq} are derived from the previous equation as follows:

$$\begin{cases} V_{rq}^{eq} = -\dot{P}_s^{ref} \frac{\sigma L_r L_s}{M V_s} + R_r I_{rq} \\ V_{rd}^{eq} = -\dot{Q}_s^{ref} \frac{\sigma L_r L_s}{M V_s} + R_r I_{rd} \end{cases} \quad (28)$$

Consequently, the switching term may be expressed as follows:

$$\begin{cases} V_{rq}^n = -K_{V_{rq}} \text{sign}(s(P_s)) \\ V_{rd}^n = -K_{V_{rd}} \text{sign}(s(Q_s)) \end{cases} \quad (29)$$

The system's stability condition can only be checked if the parameters $K_{V_{rq}}$ and $K_{V_{rd}}$ are positive.

D. Sliding Mode Control with Fuzzy Logic

1) Context of fuzzy logic sets

Type-2 fuzzy sets (T2-FSs) enhance the representation of imprecision and uncertainty. In 1975, Zadeh introduced "fuzzy fuzzy" sets, characterized by their degree of fuzziness, represented by type-1 fuzzy sets (T1-FSs) (Zadeh, 1988; Karnik and Mendel, 1998). Mendel and Liang (Liang and Mendel, 2000; Tan and Chua, 2007) introduced innovative methods for constructing T2-FSs that utilize superior and inferior membership functions (MFs), both of which can be expressed through T1-FS membership functions. The footprint of uncertainty (FOU) refers to the area bounded by these functions, which define T2-FSs.

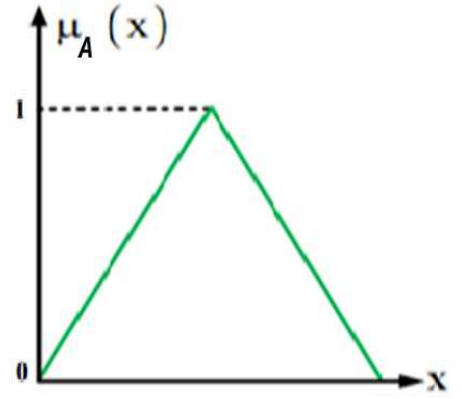
One of the key distinctions of IT2-FLC from T1-FLC is the variety of reduction processes it employs (Mendel, 2000; Mendel and John, 2001).

Figure 2 illustrates the members of Type-1 and Type-2

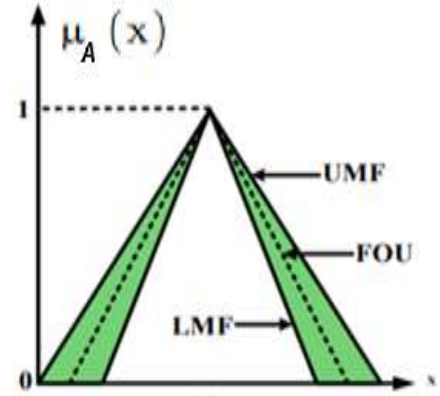
triangles. Below is a description of the Type-1 MF (Fig. 2 (a)):

$$A = (x, \mu_A(x)) \quad / x \in X \quad (30)$$

Where $\mu_A(x)$ ranges from 0 to 1, indicating the membership level of variable x in set A . Since each variable's membership level is between 0 and 1, uncertainty cannot be precisely represented. A type-2 membership function is necessary when the degree of membership of a variable is uncertain and cannot be determined (Mendel, 2000).



(a)



(b)

Figure 2: (a) Type-1 MF, (b) Type-2 MF.

The following equations explain the T2-FS shown in Fig 2 (b) and allow its expression (Milles et al., 2024):

$$\tilde{A} = \{(x, u, (\mu_{\tilde{A}}(x, u))) \mid \forall x \in X, \forall u \in J_x \subseteq [0, 1]\} \quad (31)$$

$$\tilde{A} = \int_{x \in X} \int_{u \in J_x} 1 / \mu_{\tilde{A}}(x, u) J_x \subseteq [0, 1] \quad (32)$$

When J_x is a real number between 0 and 1, the union of all valid values of x and u is shown by the double integral.

The uncertainty about (\tilde{A}) , represented by the Fou of (\tilde{A}) , is the sum of all the primary memberships, as illustrated in Fig 2. (b) (Li et al., 2023; Magaji et al., 2022).

$$FOU(\tilde{A}) = \cup_{x \in X} J_x = \{(x, u); u \in J_x \subseteq [0, 1]\} \quad (33)$$

Figure 3 illustrates the overall structure of IT2-FLCs, which is very similar to that of T1-FLCs. The main difference is that an IT2-FLC is part of the rule base, which requires a type reducer to convert the outputs of IT2-FLCs to T1-FLCs (Hassani and Zarei, 2015). The structures of IT2-FLCs include:

- The fuzzifier, similar to the process in a type-1 fuzzy logic system (T1-FLS), converts sharp input vectors (e_1, e_2, \dots, e_n) into a type-2 fuzzy system \tilde{A}_x .
- The knowledge base, which contains the human understanding of the control problem, is expressed by linguistic rules. Knowledge is transformed into logical relationships to form rule bases. These rules can be summarized as follows:

$$\text{If } e_1 \text{ is } \bar{F}_1^i \text{ and If } e_2 \text{ is } \bar{F}_2^i \text{ If } e_n \text{ is } \bar{F}_n^i, \text{ then } y^i = \tilde{G}^i, i=1, \dots, M(34)$$

- An inference engine that transforms fuzzy control inputs based on the knowledge base.
- Type reduction After the rotation and inference rules are established, the fuzzy type-2 set can be converted to a type-1 set using various reduction methods, such as joint center, sum center, height, etc. (Castillo and Melin, 2012; Castillo et al., 2012; Lathamaheswari et al., 2020).
- For the T1-FLC to produce readable output, the type-reduced set must be defuzzified.

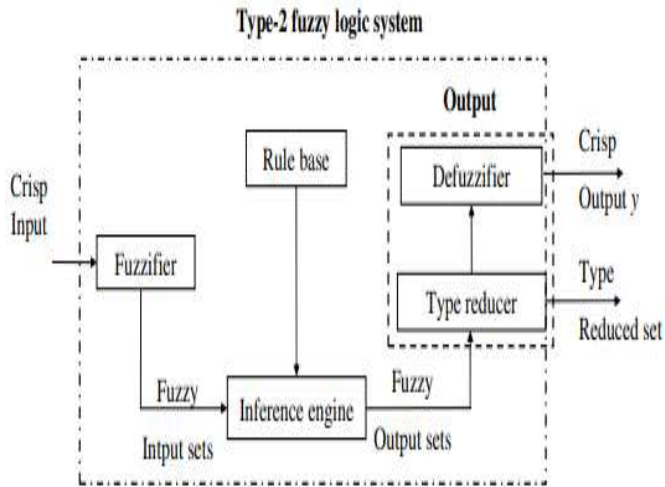


Figure 3: IT2- FLS configuration (Mendel, 2000).

2) Fuzzy sliding mode control of a DFIG

Chattering is one of the well-known issues with SMC. To increase performance and address this issue, Figure 4 depicts the recommended method, which blends fuzzy logic control with sliding mode control. This system's stability and robustness are guaranteed by merging these two solutions. Fuzzy logic control eliminates chattering.

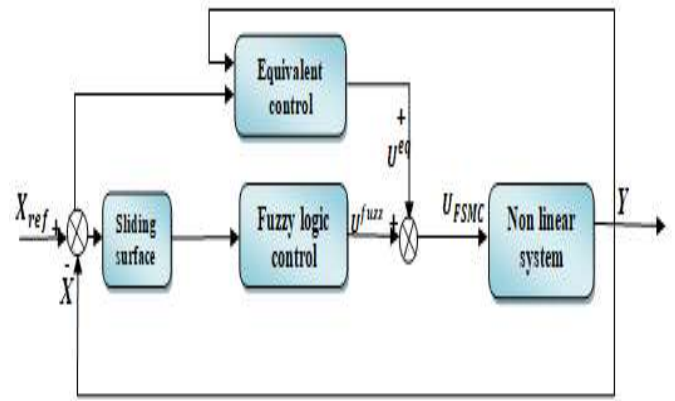


Figure 4: SMC-FLC hybrid control diagram.

III. METHODOLOGY

Figure 5 depicts the detailed framework of the control strategy proposed. Substituting the switching controller term $(K_{sing}(s))$ with a fuzzy control input (IT2-FLC and T1-FLC) transforms the sliding mode controller (eqn. (19)) into the fuzzy sliding mode controller (FSMC).

$$u = u^{eq} + u^{fuzzy} \quad (35)$$

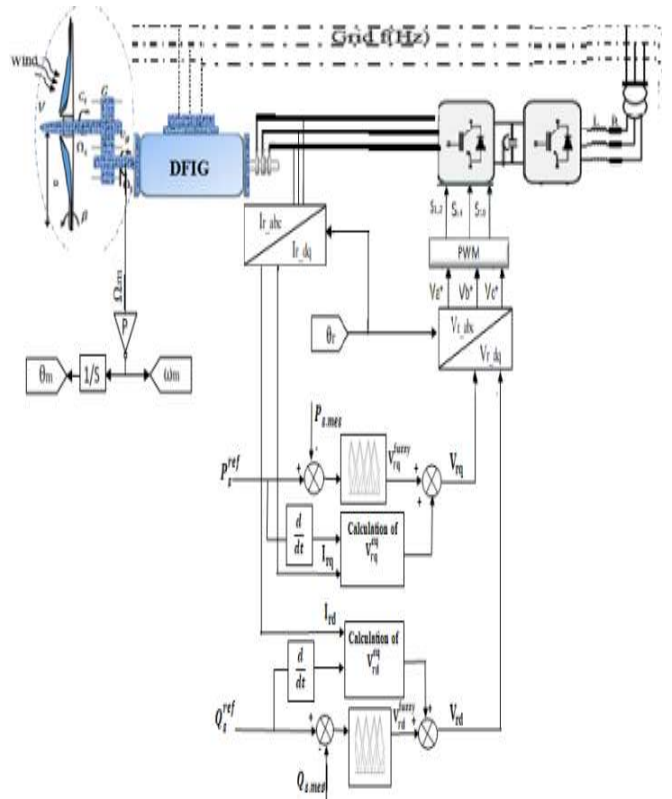


Figure 5: Control of the IT2-FSMC

This article selected five triangular membership functions for the IT2-FLC and T1-FLC due to their ease of implementation in hardware. Figures 6 and 7 illustrate the inputs and outputs. The discourse universe for all inputs and outcomes ranged from -1 to +1.

IV. SIMULATION RESULTS

In this simulation segment, a 10 kW generator is connected to a 400V/50 Hz network, with system parameters detailed in the appendix. To compare the T1FSMC and IT2FSMC controllers, two tests were conducted: a tracking test and a robust test against variations in machine parameters.

A. First test

This section verifies the techniques proposed for enhancing the generator's performance under optimal conditions, specifically without disturbances or adjustments to the machine parameters.

Figure 08 shows a wind speed of approximately 10 m/s. When the wind speed is below the nominal speed, the wind turbine system operates in Maximum Power Point Tracking (MPPT) mode, generating power at its maximum capacity. When the wind speed exceeds the nominal speed, the system controller adjusts the turbine rotation to maintain the electrical power output at the nominal value during the interval [1.7 s, 3.2 s]. The power generated is significantly affected by even small changes in wind speed, as it is directly proportional to the cube of the wind speed. The negative sign of P_s indicates that the DFIG generated power and transmitted it to the grid. The reactive power response was reduced to zero from 0 to 2.3 seconds to achieve uniform power factor operation, as shown in Figure 09(b). The performance achieved with the T1FSMC and IT2FSMC controllers is highly satisfactory, as demonstrated by the tracking and extremely fast convergence of the measured variables to the target reference, as shown in Figure 09. The use of this method made it possible to achieve perfect decoupling between the two components of the stator power.

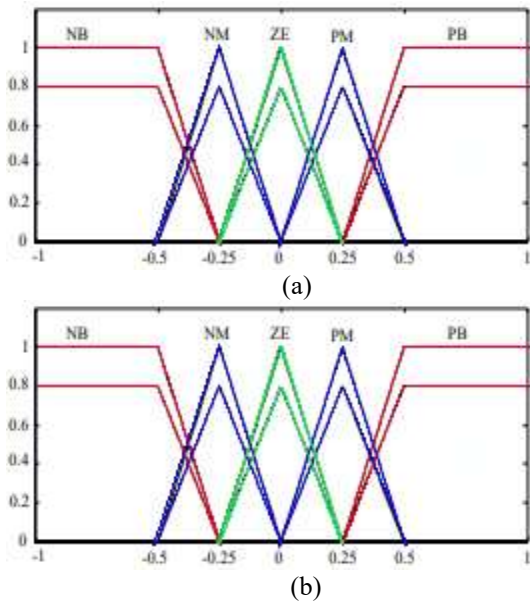


Figure 6: IT2-FLC membership functions for input and output

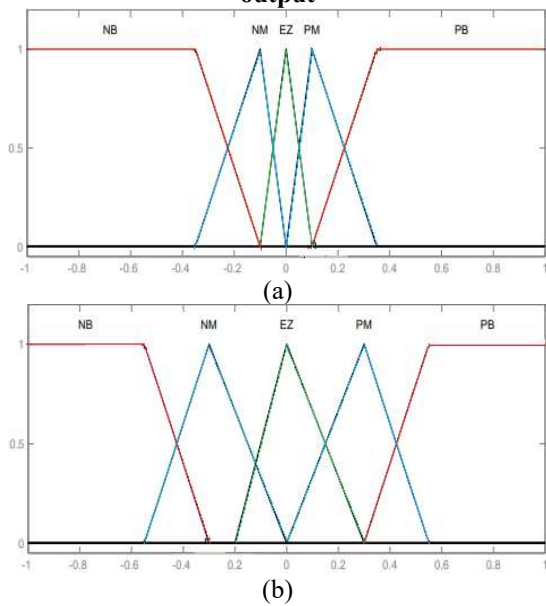


Figure 7: T1-FLC membership functions for input and output

To ensure the optimal performance of the controllers, Table 1 summarizes the IT2-FLC and T1-FLC rule bases. The rule base is the framework around which the IT2-FLC and T1-FLC are built, drawing on process dynamics as well as the knowledge and experience of experts.

Table 1: Base tables for fuzzy logic control rules

Fuzzy input	NB	NM	EZ	PG	PB
Fuzzy output	NB	NM	EZ	PG	PB

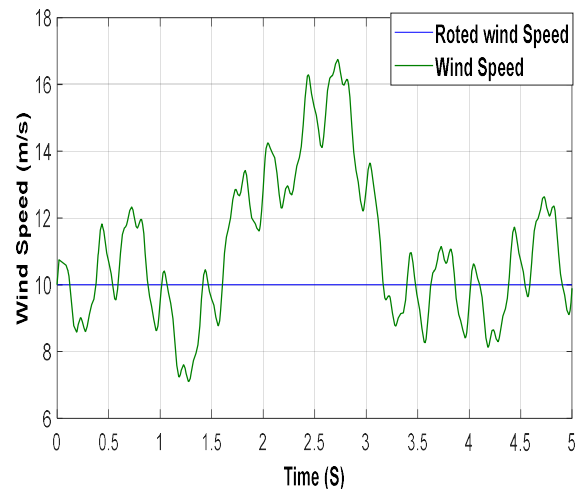
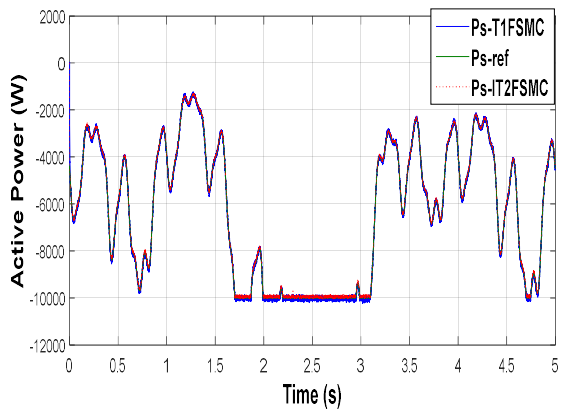
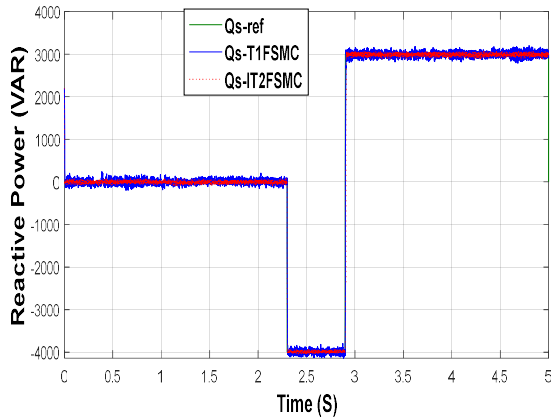


Figure 8: Wind speed (V) profile



(a)

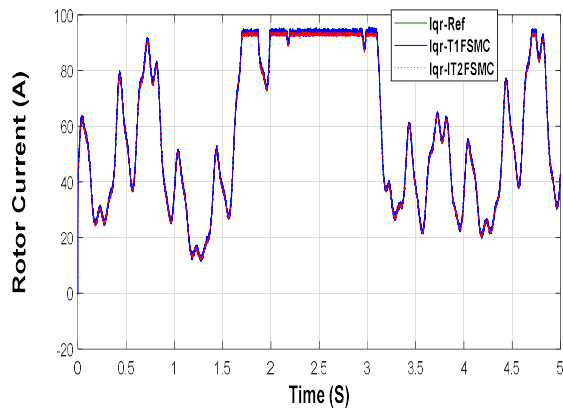


(b)

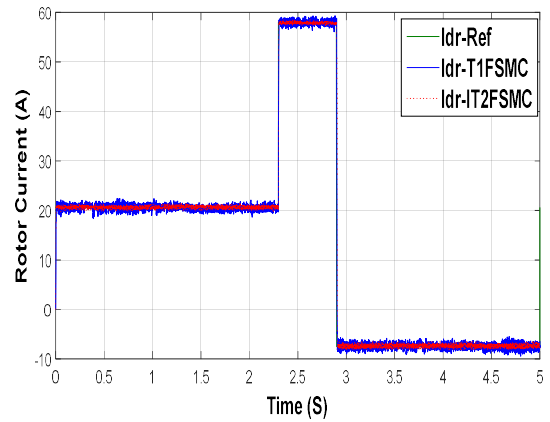
Figure 09: (a) Active power (P_s); (b) reactive power (Q_s)

Figure 10 illustrates the rotor current components along the d- and q-axes, representing the stator's reactive and active power. Notably, the rotor currents followed the reference trajectories without any overshoot.

Figure 11. (a) illustrates the sinusoidal waveform of stator currents at 50 Hz, varying with wind speed. In contrast, Figure 11. (b) displays the rotor circuit currents as sinusoidal waves, with their frequency and magnitude dependent on slip or generator speed.

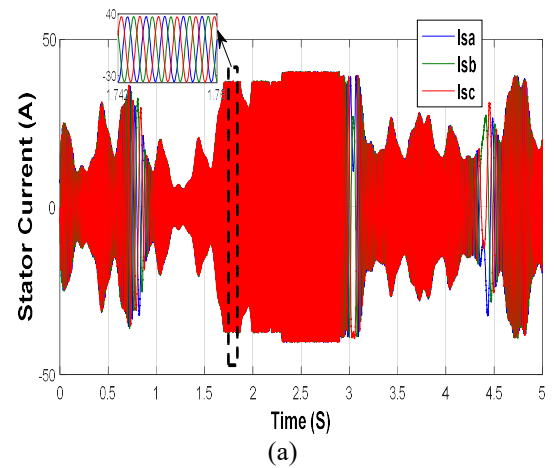


(a)

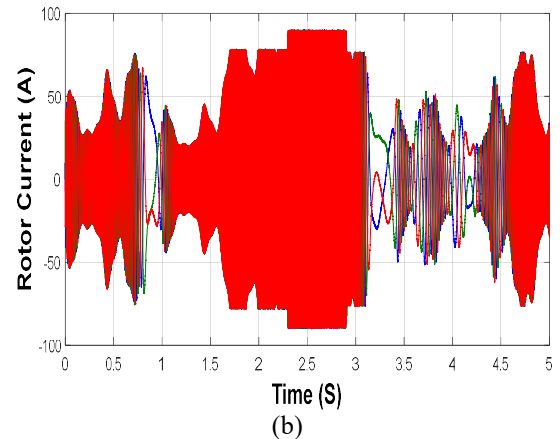


(b)

Figure 10: (a) rotor current (I_{qr}); (b) rotor current (I_{dr}).



(a)



(b)

Figure 11: (a) stator current; (b) rotor current.

Figure 12 shows that the DFIG's One-Phase Stator Current Harmonic Spectrum was measured using the Fast Fourier Transform (FFT) method for both controllers. Comparing (IT2-FSMC, THD = 2.52% vs. T1-FSMC, THD = 3.26%), the decrease in total harmonic distortion (THD) is evident. Thus, the IT2-FLC method significantly reduced THD, with an estimated reduction ratio of 22.69%.

This percentage indicates that the present quality is higher with the IT2-FSMC method than the T1-FSMC method. Additionally, the IT2-FSMC command yielded a higher basic signal amplitude (50 Hz) than the T1-FSMC method.

These results indicate that the IT2-FSMC method surpasses the T1-FSMC method.

efficient when considering the energy criterion, as shown in Table 2.

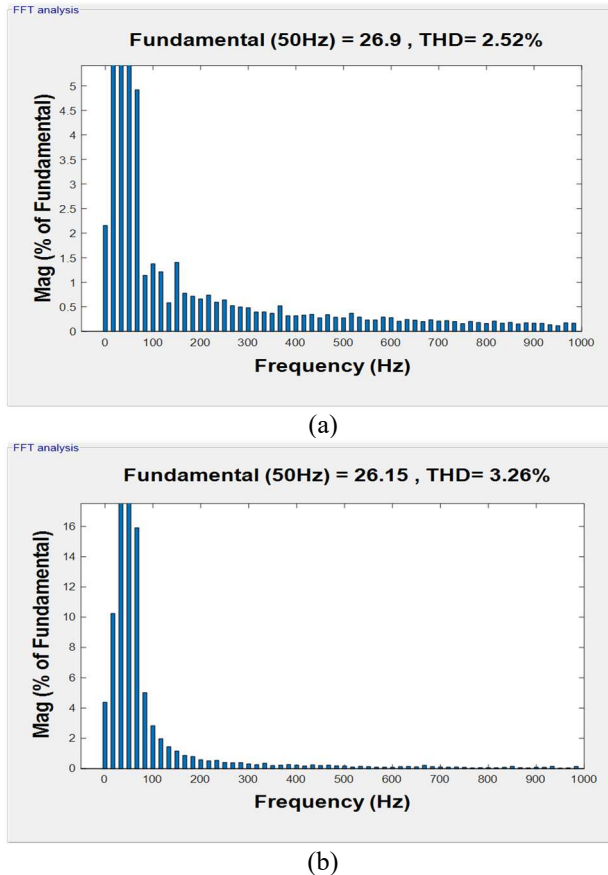


Figure 12: (a) THD IT2-FSMC; (b) THD T1-FSMC

B. Robustness test

This section evaluates the robustness and performance of the IT2-FSMC controller under adverse variations in control system parameters due to phenomena like inductance saturation and resistance heating, as well as wind speed disturbances. The findings are compared with the T1-FSMC approach. The test involves modifying the generator's internal parameters to assess the IT2-FSMC's robustness and reaction speed to uncertainties compared to the T1-FSMC. The stator and rotor resistance (R_r, R_s) are doubled, the stator and rotor inductors (L_s, L_r) are adjusted to 30% of their nominal values, and M is reduced to 50% of its initial value.

The test results are displayed in Figure 13 and Table 2. In comparison to the T1-FSMC method, the IT2-FSMC strategy provides more accurate Q_s and P_s that closely match the references. Additionally, the IT2-FSMC shows significantly faster response times and lower power ripples compared to the T1-FSMC controller. The performance of simulations using this controller type, including reference tracking (time response, overshoot), sensitivity to disturbances, and overall effectiveness, was notably intriguing.

Table 2 shows the values and reduction ratios for the controls utilized when the machine parameters change, including rise time, ISE , IAE , $ITSE$, and $ITAE$. It is clear from the comparison that the IT2-FSMC controller produces better results than the T1-FSMC. The control IT2-FSMC is the most

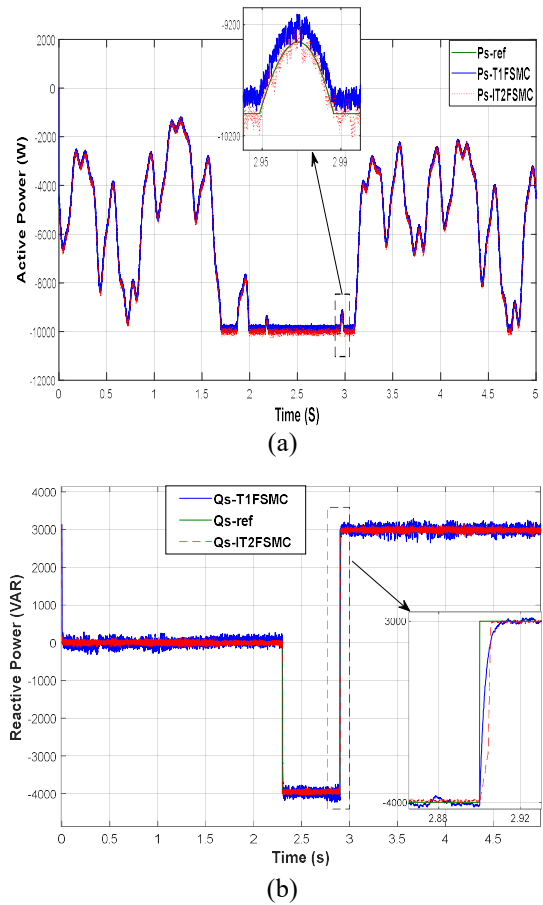


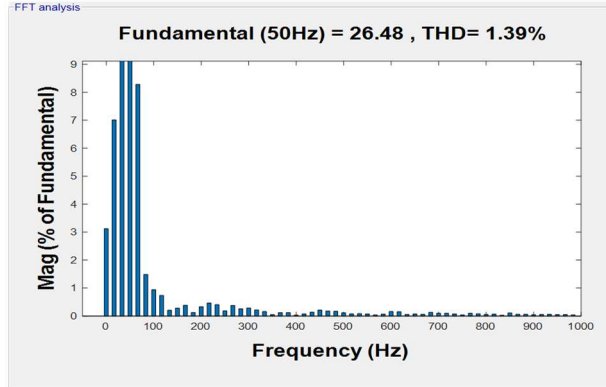
Figure 13: (a) Active power (P_s); (b) reactive power (Q_s)

Table 2: Numerical results from the robustness test

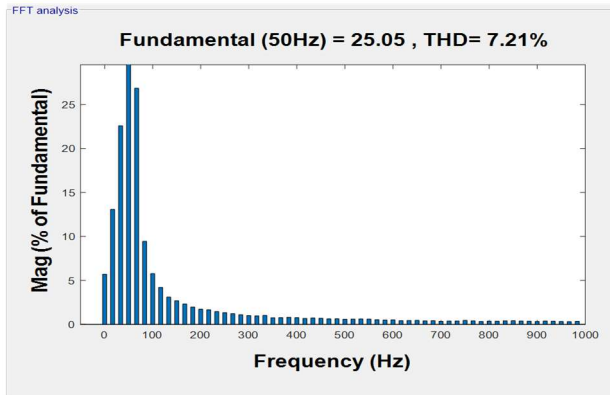
	IAE	ITAE	ISE	ITSE	Rise Time (sec)
P_s (T1-FSMC)	411.5	1027	5.048e4	9.818e4	0.006
P_s (IT2-FSMC)	291	705.7	4.424e4	4.111e4	0.002
Ratio	29.28 %	31.28 %	12.36 %	58.12 %	66.66 %
Q_s (T1-FSMC)	348.9	851.1	1.699e5	4.813e5	0.0065
Q_s (IT2-FSMC)	183.7	416.8	1.182e5	2.825e5	0.0015
Ratio	47.34 %	51.02 %	30.42 %	41.30 %	76.92 %

Figures 14(a) and (b) depict the current THD values under different control methods. Using the T1-FSMC method, the current THD was 7.21%, whereas with the IT2-FSMC method, it was reduced to 1.39%. The IT2-FSMC method improved current quality and reduced current ripples by 80.72% compared to the T1-FSMC method (see Table 5). Additionally, while utilizing the IT2-FSMC method, the amplitude of the

basic (50 Hz) current signal was 26.48 A, whereas when using the T1-FSMC method, it was 25.05 A. This demonstrates that the IT2-FSMC method outperforms the T1-FSMC method. Accordingly, the simulation results display that the controller (IT2-FSMC) is the superior option when dealing with parameter fluctuations and uncertainty in disturbances to the system.



(a)



(b)

Figure 14: (a) THD IT2-FSMC; (b) THD T1-FSMC

Table 3: The current THD values between the two tests.

	THD % (Test 1)	THD % (Test 2)
T1-FSMC	3.26	7.21
IT2-FSMC	2.52	1.39
Ratio	22.69%	80.72%

V. Conclusions

This study evaluates the efficacy of a Doubly Fed Induction Generator's (DFIG) active and reactive power control using hybrid fuzzy sliding mode control. After explaining the DFIG's operation with fixed grid frequency and variable wind speed, we developed a mathematical model for its two-phase power to manage energy and reactive power flows between the grid and the DFIG, the implementation of the IT2-FSMC approach using Matlab software will be utilized to compare the outcomes with the control based on the T1-FSMC technique. The system was then subjected to two distinct scenarios that tested its resilience: disruptions caused by extremely high wind

speeds and variations in system parameters. Visual comparisons reveal that the IT2-FLC approach is more effective and delivers better outcomes than T1-FLC. Adding error reduction ratios and ripples in reactive and active power, we may conclude that altering system parameter values affects current quality, as represented by total harmonic distortion. The IT2-FLC technique has less impact than the T1-FLC method.

Robust controllers will be the primary emphasis of future studies. To manage a variable-speed wind turbine that uses a DFIG, we are creating a smart hybrid controller that combines IT2-FLC with a backstepping control method.

APPENDIX Parameters of the model.

Parameters	Value
Rated power	10 kW
Stator voltage	230/400 V
Frequency	50 Hz
Rs (Stator resistance)	0.455 Ω
Rr (Rotor resistance)	019 Ω
Ls (Stator inductance)	0.07 H
Lr (Rotor inductance)	0.0213 H
M (Mutual inductance)	0.034 H
P (Number of pole pairs)	2
ρ (Air density)	1.225Kg/m ³
R _b (Blade radius)	3.45m
Hm (Inertia constant)	2s
D (Damping coefficients)	0.01Nm.s/rad

AUTHOR CONTRIBUTIONS

I. Allali: Conceptualization, Software, Validation, Writing – original draft, review & editing. **B. Dehiba:** Conceptualization, Methodology, Supervision, Writing – review & editing.

REFERENCES

- Acikgoz, H., Kececioglu, O., Gani, A., Tekin, M., & Sekkeli, M. (2017).** Robust control of shunt active power filter using interval type-2 fuzzy logic controller for power quality improvement. *Tehnicki Vjesnik-Technical Gazette*, 24.
- Adeyanju, A. A. (2023).** The Influence Of Rotor Separation On The Performance Of A Dual-Rotor Wind Turbine. *Journal of Namibian Studies, History Politics Culture*, 35, 4684-4702.
- Amira, L., Tahar, B., & Abdelkrim, M. (2020).** Sliding mode control of doubly-fed induction generator in wind energy conversion system. *In 2020 8th International Conference on Smart Grid (icSmartGrid)*. (pp. 96-100). IEEE.
- Bühler, H. (1986).** Sliding mode adjustment. EPFL Press.
- Castillo, O., & Melin, P. (2012).** A review of the design and optimization of interval type-2 fuzzy controllers. *Applied Soft Computing*, 12(4), 1267-1278.
- Castillo, O., Martinez-Marroquin, R., Melin, P., Valdez, F., & Soria, J. (2012).** Comparative study of bio-inspired algorithms applied to the optimization of type-1 and

type-2 fuzzy controllers for an autonomous mobile robot. *Information sciences*, 192, 19-38.

Chakib, M., Nasser, T., & Essadki, A. (2020). Comparative study of active disturbance rejection control with RST control for variable wind speed turbine based on doubly fed induction generator connected to the grid. *International Journal of Intelligent Engineering and Systems*, 13(1), 248-258.

Hassani, H., & Zarei, J. (2015). Interval Type-2 fuzzy logic controller design for the speed control of DC motors. *Systems Science & Control Engineering*, 3 (1), 266-273.

Heier, S. (2014). Grid integration of wind energy: onshore and offshore conversion systems. *John Wiley & Sons*.

Hemeyine, A. V., Abbou, A., Tidjani, N., Mokhlis, M., & Bakouri, A. (2020). Robust Takagi Sugeno fuzzy models control for a variable speed wind turbine based on a DFIG. *International Journal of Intelligent Engineering and Systems*, 13(3), 90-100.

Kadri, A., Marzougui, H., Aouiti, A., & Bacha, F. (2020). Energy management and control strategy for a DFIG wind turbine/fuel cell hybrid system with super capacitor storage system. *Energy*, 192, 116518.

Kaloi, G. S., Baloch, M. H., Kumar, M., Soomro, D. M., Chaudhary, S. T., Memon, A. A. & Ishak, D. (2019). An LVRT scheme for grid-connected DFIG based WECS using state feedback linearization control technique. *Electronics*, 8(7), 777.

Karnik, N. N., & Mendel, J. M. (1998, May). Introduction to type-2 fuzzy logic systems. In 1998 IEEE International Conference on Fuzzy Systems proceedings. *IEEE World Congress on computational intelligence* (Cat. No. 98CH36228) (Vol. 2, pp. 915-920). IEEE.

Khan, D., Ahmed Ansari, J., Aziz Khan, S., & Abrar, U. (2020). Power optimization control scheme for doubly fed induction generator used in wind turbine generators. *Inventions*, 5(3), 40.

Kheir Saadaoui, B. B., Assas, O., & Khodja, M. A. (2019). Type-1 and type-2 fuzzy sets to control a nonlinear dynamic system. *Revue d'Intelligence Artificielle*, 33(1), 1-7.

Lathamaheswari, M., Nagarajan, D., Kavikumar, J., & Broumi, S. (2020). Triangular interval type-2 fuzzy soft set and its application. *Complex & Intelligent Systems*, 6, 531-544.

Li, K., Zhang, X., Han, Y. (2023). Robot path planning based on interval type-2 fuzzy controller optimized by an improved Aquila optimization algorithm. *IEEE Access*.

Liang, Q., & Mendel, J. M. (2000). Interval type-2 fuzzy logic systems: theory and design. *IEEE Transactions on Fuzzy Systems*, 8(5), 535-550.

Magaji, N., Mustafa, M.W.B., Lawan, A.U., Tukur, A., Abdullahi, I., Marwan, M., (2022). Application of Type 2 fuzzy for maximum power point tracker for photovoltaic system. *Processes* 10 (8), 1530.

Mancini, M., Capello, E., & Punta, E. (2020). Sliding mode control with chattering attenuation and hardware constraints in spacecraft applications. *IFAC-PapersOnLine*, 53(2), 5147-5152.

Mendel, J. M. (2000). Uncertainty, fuzzy logic, and signal processing. *Signal Processing*, 80(6), 913-933.

Mendel, J. M., & John, R. I. (2001, July). A fundamental decomposition of type-2 fuzzy sets. In *Proceedings joint 9th IFSA world congress and 20th NAFIPS international conference* (Cat. No. 01TH8569) (Vol. 4, pp. 1896-1901). IEEE.

Milles, A., Merabet, E., Benbouhenni, H., Debdouche, N., & Colak, I. (2024). Robust control technique for wind turbine system with interval type-2 fuzzy strategy on a dual star induction generator. *Energy Reports*, 11, 2715-2736.

Mousa, H. H., Youssef, A. R., & Mohamed, E. E. (2020). Hybrid and adaptive sectors P&O MPPT algorithm based wind generation system. *Renewable Energy*, 145, 1412-1429.

Mousavi, Y., Bevan, G., Kucukdemiral, I. B., & Fekih, A. (2022). Sliding mode control of wind energy conversion systems: Trends and applications. *Renewable and Sustainable Energy Reviews*, 167, 112734.

Okedu, K. E., Al Tobi, M., & Al Araimi, S. (2021). Comparative study of the effects of machine parameters on DFIG and PMSG variable speed wind turbines during grid fault. *Frontiers in Energy Research*, 9, 681443.

Sahri, Y., Tamalouzt, S., Lalouni Belaid, S., Bacha, S., Ullah, N., Ahamdi, A. A. A., & Alzaed, A. N. (2021). Advanced fuzzy 12 dtc control of doubly fed induction generator for optimal power extraction in wind turbine system under random wind conditions. *Sustainability*, 13(21), 11593.

Scarabaggio, P., Grammatico, S., Carli, R., & Dotoli, M. (2021). Distributed demand side management with stochastic wind power forecasting. *IEEE Transactions on Control Systems Technology*, 30(1), 97-112.

Shuaibu, M., Abubakar, A. S., & Shehu, A. F. (2021). Techniques for ensuring fault ride-through capability of grid connected dfig-based wind turbine systems: a review. *Nigerian Journal of Technological Development*, 18(1), 39-46.

Slotine, J. J. E. (1991). Applied nonlinear control. *PRENTICE-HALL google schola*, 2, 1123-1131

Tan, W. W., & Chua, T. W. (2007). Uncertain rule-based fuzzy logic systems: introduction and new directions (Mendel, JM; 2001)[book review]. *IEEE Computational Intelligence Magazine*, 2(1), 72-73.

Xiong, L., Li, J., Li, P., Huang, S., Wang, Z., & Wang, J. (2021). Event triggered prescribed time convergence sliding mode control of DFIG with disturbance rejection capability. *International Journal of Electrical Power & Energy Systems*, 131, 106970.

Yan, S. R., Dai, Y., Shakibjoo, A. D., Zhu, L., Taghizadeh, S., Ghaderpour, E., & Mohammadzadeh, A. (2024). A fractional-order multiple-model type-2 fuzzy control for interconnected power systems incorporating renewable energies and demand response. *Energy Reports*, 12, 187-196.

Yin, M., Xu, Y., Shen, C., Liu, J., Dong, Z. Y., & Zou, Y. (2016). Turbine stability-constrained available wind power of variable speed wind turbines for active power control. *IEEE Transactions on Power Systems*, 32(3), 2487-2488.

Zadeh, L. A. (1988). Fuzzy logic. *Computer*, 21(4), 83-93.